Wear Debris Classification and Quantity and Size Calculation Using Convolutional Neural Network

Hongbing Wang[1], Fei Yuan[2,3(✉)], Liyuan Gao[1], Rong Huang[1], and Weishen Wang[1]

[1] School of Computer and Communication Engineering, University of Science and Technology Beijing, Beijing 100083, China
[2] School of Metallurgical and Ecological Engineering, University of Science and Technology Beijing, Beijing 100083, China
yuanfei@ustb.edu.cn
[3] State Key Laboratory of Advanced Metallurgy, University of Science and Technology Beijing, Beijing 100083, China

Abstract. The steel production equipment faults are mostly caused by wear faults, and the classification of wear debris in its lubrication system can monitor the wear status of the machine. The traditional methods of wear debris image classification mostly use digital image processing technology by extracting color, shape, texture and other multi-dimensional features of wear debris. It is so difficult to extract suitable multi-dimensional features that the classification accuracy is always kept at a low level. Convolutional Neural Network can directly take the image pixels as input, and extract features automatically, avoiding the poor applicability of manual extraction methods and complicated image pre-processing. An improved lightweight convolutional neural network for wear debris image classification named UstbNet is proposed in this paper. Data augmentation, number and size adjustment of convolution kernels, batch normalization and loss function optimization are used to speed up the model convergence and improve the classification accuracy. The classification accuracy of UstbNet model reaches 96%. After the step of determining the existence of wear debris, we use Faster RCNN to detect the quantity and size of wear debris and further improve it. Grabcut is applied to segment wear debris image based on detected region proposals.

Keywords: Convolutional Neural Network · Wear debris · Classification · Faster RCNN · Grabcut

1 Introduction

Wear debris are the friction particles suspended in the oil of lubrication system, produced by internal friction pair wear of equipment [1]. They carry a great deal of information about the running status of a machine. The state of wear debris can reveal the wear degree and wear mechanism, providing an important reference to improve the working condition of machines such as rolling mill, aircraft engines and marine engines

The original version of this chapter was revised: The values in Table 10 have been modified. The correction to this chapter is available at https://doi.org/10.1007/978-981-15-1922-2_42

H. Ning (Ed.): CyberDI 2019/CyberLife 2019, CCIS 1137, pp. 470–486, 2019.
https://doi.org/10.1007/978-981-15-1922-2_33

[2]. The wear status of a machine can be checked by extracting wear debris information, and different types of wear debris correspond to different faults. In the metallurgical rolling production process, mill gears as a carrier of power and torque transmission, have a direct impact on the normal operation of mechanical systems and rolled steel [3–6]. Abrasion is the main cause of machine failure, and the equipment wear curve is shown in Fig. 1. Common types of wear debris in lubricating oil are shown in Fig. 2. The wear debris generated in the oil film bearing and the corresponding failure are shown in Table 1. The classification of wear debris can reflect the wear condition of the oil film bearing, so as to maintain the oil film bearing in time.

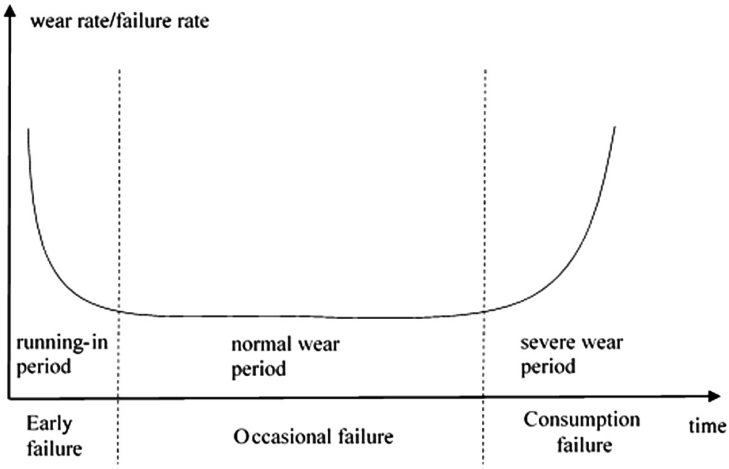

Fig. 1. Equipment wear curve

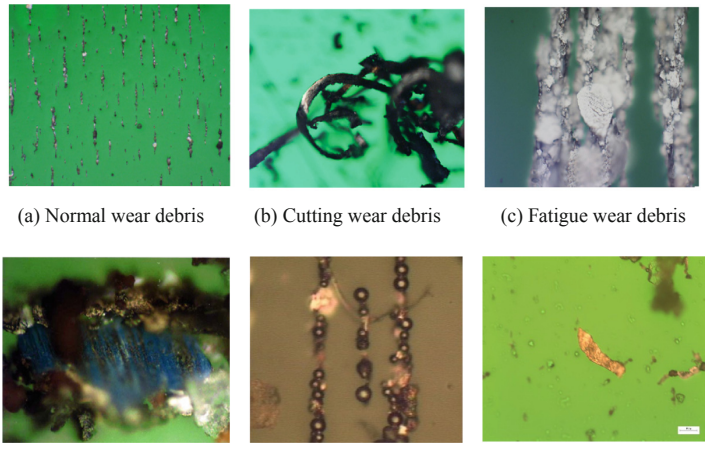

Fig. 2. Typical wear debris

Table 1. Wear debris and their faults in the oil film bearing

Wear debris type	Fault form
Cutting and Black oxide wear debris	Surface friction of bolster bearing
Cutting wear debris of non-ferrous metals	Surface friction of oil film bearing
Fatigue wear debris	Shedding of bushing surface
Severe sliding wear debris	Insufficient lubrication

Wear debris analysis and identification are mainly accomplished by domain experts at early stage, with high cost and a lot of time. In recent years, the rapid development of computer and artificial intelligence have promoted the automatic analysis and recognition of wear debris [7]. Thomas and Stachowiak analyzed the variable scale and fractal features of wear debris [8, 9]. Their researches focus on the digitalization of wear debris features. Roylance pioneered the computer wear debris pattern recognition research direction. He tried to use the grayscale value of different metal wear debris to identify the components, but the classification result is not good [10]. Xu and Luxmoore developed a neural network and expert system integrated interactive automatic identification system for wear debris, but the input features of neural network need to be extracted manually [11]. Zuo compared the application of BP (Back Propagation) neural network, fuzzy BP and gray fixed weight clustering in the recognition of wear debris [12]. Li took ELM (Extreme Learning Machine) as classifier, the shape, color and texture feature of wear debris as input [13]. However, the feature extraction is done manually and the wear debris image needs to be preprocessed.

Many image classification algorithms have been proposed [14–18]. However, the classification of wear debris must be based on multi-dimensional features. Most of the above studies focus on only a few features of color, shape or texture, and the low classification accuracy could be achieved [19–22]. The multi-dimensional feature extraction is difficult by using various conventional and single models. Convolutional Neural Network (CNN) can learn the features from bottom to top automatically from massive images, and lead the result of image classification close to human level. CNN has been proved to be very effective for general object classification tasks [23–28]. In this paper, we construct an improved lightweight CNN for wear debris image classification named UstbNet and get better result for wear debris detection through the improved Faster RCNN.

The remainder of the paper is organized as follows. In Sect. 2, a new CNN we develop for classifying wear debris images is presented and experimental results are shown and discussed. Wear debris quantity and size are analyzed in Sect. 3. We introduce the application of the classification model UstbNet in steel production equipment in Sect. 4 and a conclusion is presented in Sect. 5.

2 Wear Debris Image Classification

2.1 Convolutional Neural Network Structure

CNN is a multi-layer neural network, it has a high degree of invariance to image distortion, and can take massive images as input directly to produce many features. The typical CNN mainly includes input layer, convolutional (conv) layer, pooling layer, norm layer, full connected layer, logistic regression layer and output layer. CNN reduces the dimensionality of image features by weight sharing, local perception and subsampling, so that the network can be trained and complexity is reduced.

The usual CNN include Cifar10, AlexNet and GoogleNet. Cifar10 is a simple network designed for databases based on 10 categories. AlexNet and GoogleNet have all achieved high classification accuracy on large dataset ImageNet, but their network structures are complex, and these networks require a lot of time to train the model.

In this paper, we proposed an improved lightweight CNN named UstbNet. Data augmentation, number and size adjustment of convolution kernels, batch normalization and loss function optimization are used to speed up the model convergence and improve the classification accuracy. The model used for training consists of nine layers, out of which six are conv layers and three are fully connected layers, as depicted in Fig. 3. The kernel size and kernel number of each conv layer and the number of neurons in fully-connected layer are listed in the following Table 2.

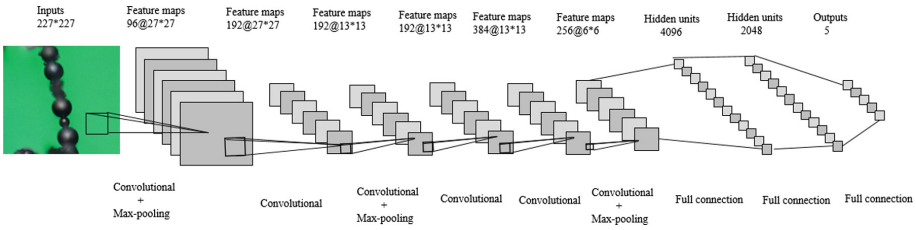

Fig. 3. Convolutional neural network UstbNet

Table 2. UstbNet network parameter description

Layer	Kernel size	Kernel/Neuron number	Stride
Conv1 + Relu	11	96	4
Pool + BachNorm+Scale	3	–	2
Conv2	3	192	1
Conv3 + Relu	3	192	1
BachNorm+Scale + Pool	3	–	2
Conv4 + Relu	3	192	1
Conv5 + Relu	3	384	1
Conv6 + Relu	3	256	1
Pool	3	–	2
FC1	–	4096	–
FC2	–	2048	–
FC3(Output)	–	5	–

2.2 Experimental Results and Comparisons

2.2.1 Data Augmentation

The traditional data augmentation methods include several types of transformation: rotation, skew, rescaling, flipping, shearing and add noisy. The settings for these transformations used in the experiment are presented in Table 3. The original dataset increased from 1640 to 8370 through data augmentation. To get a clear idea for different types of transformation, the transformed images for the same image with different methods are shown in Fig. 4.

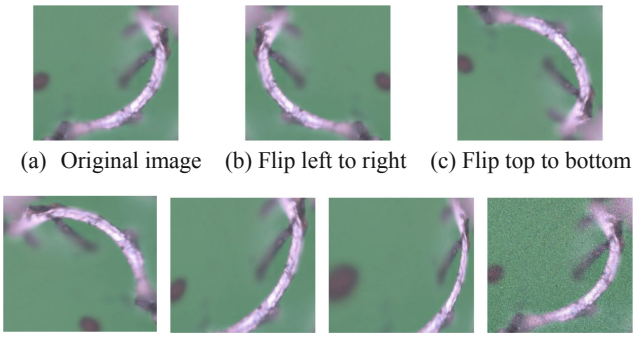

Fig. 4. The view of different types of transformation

Table 3. Parameter setting for data augmentation method

Method	Settings
Rotation	Random with angle in [0°, 360°]
Rescaling	Random crop to 227 * 227
Flipping	Left to right
Flipping	Top to bottom
Shearing	Random with angle [−25°, 25°]
Skew	Random with magnitude 0.8
Add Noise	Gaussian

2.2.2 Experimental Configuration

All experiments in this study are performed on a desktop computer with i7-6700 (3.40 GHz), 16 GB RAM, NVIDIA GeForce GTX 1060 6G GPU. The train parameters are as follows: the learning rate is set to 0.001 with fixed policy, momentum: 0.9, weight decay: 0.0005, max iterations: 10000, and the mini-batch gradient descent method is used for parameter updating.

The experimental images are provided by a steel plant. The wear debris on ferrography are often overlapped with each other, so it is necessary to divide them for constructing the image database with single type wear debris. The size and shape of

each image are different due to the different shooting angles and magnification, but the input of CNN needs the same size image. The wear debris images are unified into 256 * 256 size.

After preprocessing the images, the number of training dataset, validation dataset and test dataset for each class of wear debris images used in the experiment are shown in Table 4. In each training, the training dataset and validation dataset are divided randomly in the ratio of 4:1 in order to achieve the purpose of cross-validation.

Table 4. Number of experimental images

Wear debris classification	Training dataset	Validation dataset	Test dataset
Normal wear debris	1248	312	314
Spherical wear debris	1090	272	232
Cutting wear debris	930	232	236
Severe sliding wear debris	1011	252	302
Fatigue wear debris	1303	325	311
Total number	5582	1393	1395

2.2.3 Experimental Analysis

The basic UstbNet includes six conv layers and three fully connected layers. To investigate the behavior of Batch Normalization, SoftmaxWithLoss and Dropout as proposal methods, we conducted several ablation studies on the basic UstbNet. From Table 5, the results show that the network with SoftmaxWithLoss is more accurate than HingeLoss. Therefore, the following experiments are adopted SoftmaxWithLoss. As shown in Table 6, it is obviously that Batch Normalization can improve the classification accuracy and are better than Dropout. Dropout can reduce the training time while Batch Normalization slow down the training because of the large number of matrix operations. Furthermore, the combination of Batch Normalization and Dropout is the best.

Table 5. Ablation experiments of SoftmaxWithLoss and HingeWithLoss

Network structure	Average cross-validation accuracy (%)	Test accuracy (%)
Basic UstbNet + SoftmaxWithLoss	93.2	92
Basic UstbNet + HingeWithLoss	91	89

Table 6. Ablation experiments of Batch Normalization and Dropout

Network structure	Average cross-validation accuracy (%)	Test accuracy (%)	Average Training time (min)
Basic UstbNet + Batch Norm	95.6	94	138
Basic UstbNet + Dropout	94.2	93	113
Basic UstbNet + BatchNorm + Dropout	96.8	96	122

By using the same configuration as UstbNet, the experimental results of Cifar10, AlexNet, GooleNet and UstbNet on GPU are shown in Table 7. Both the validation accuracy and test accuracy of UstbNet are the highest. Through analyzing the accuracy and loss curve of above network structures as shown in Fig. 5, we can see that UstbNet guaranteed loss to decrease and stabilize gradually while achieving the highest accuracy. Besides, using GPU greatly speeds up the training speed and shortens the training time.

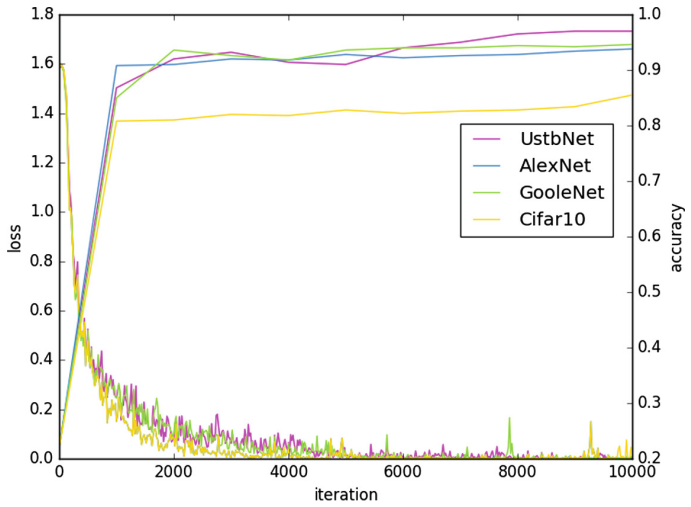

Fig. 5. The accuracy and loss curve

Table 7. Comparison of experimental results of cifar10 and UstbNet

Model	Layers	GPU training time (min)	Average cross-validation accuracy (%)	Test accuracy (%)
AlexNet	8	202	94	93.8
Cifar10	5	8	85.5	84
GoogleNet	22	78	95	94.2
UstbNet	9	122	96.8	96

3 Wear Debris Quantity and Size Calculation

The wear debris image classification is used to judge whether there are wear debris or not, and the calculation in this section is for finding out the specific type of different wear debris.

3.1 Object Detection Algorithm Faster RCNN

Faster RCNN is a CNN object detection framework, gradually developed by RCNN. Faster RCNN consists of four parts. (1) Faster RCNN first uses a set of basic CNN to extract the feature maps of image. The feature maps are shared for subsequent Region Proposal Network (RPN) and full connection layer. (2) RPN is used to generate region proposals. The layer uses softmax to determine whether anchors belong to foreground or background, and then uses bounding box regression to correct anchors to obtain accurate proposals. (3) ROI pooling collects input feature maps and proposals. After synthesizing these information, proposal feature maps are extracted and sent to the subsequent full connection layer to determine the target category. (4) The proposal feature maps are used to calculate the classification of the proposal. The final detection box is obtained by bounding box regression again.

As shown in Fig. 6, an image (P × Q) is input to Faster RCNN, scaling to a fixed size M × N after sending to the basic conv networks. RPN first performs 3x3 convolution on the feature map, then generates offset between foreground anchors and bounding box regression, and calculates proposals. The ROI pooling uses proposals to extract proposal features from feature maps and send them to subsequent full-connection and softmax to classify the proposals.

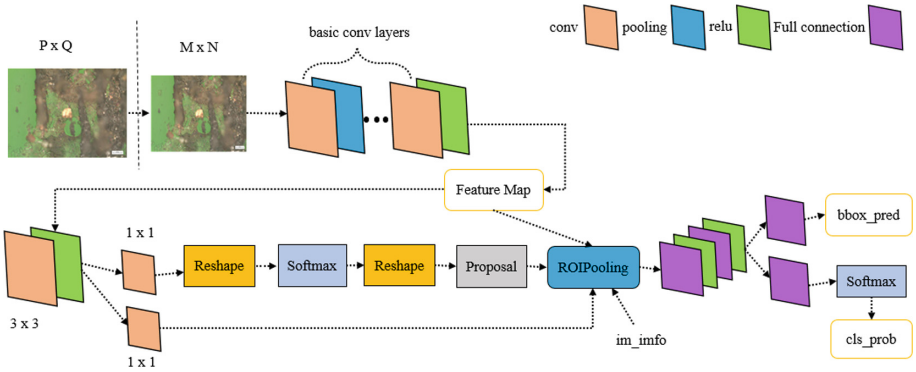

Fig. 6. Faster RCNN structure

3.2 Faster RCNN Improvement

3.2.1 Region-Based Fully Convolutional Networks R-FCN

Classification requires feature translation invariance, while detection requires accurate response to object translation. Faster RCNN are all conv layers before ROI pooling. It has translation invariance. After inserting ROI pooling, the full connection layers no longer have translation invariance and unable to share computing. Therefore, it has position translation-invariance and does not match the network's superior classification accuracy. In order to introduce translation variance, R-FCN uses a special conv layer to construct position-sensitive score maps and remove the full connection layers. R-FCN algorithm steps are shown in Fig. 7. Firstly, the preprocessed images are sent into a

pre-trained classification network. The corresponding network parameters are fixed. There are three branches on the feature map obtained from the last conv layer of the pre-trained network. One gets the corresponding ROI from the RPN operated on the feature map. Another gets a k * k * (C + 1) dimension position-sensitive score map on the feature map for the classification. A 4 * k * k dimension position-sensitive score map is obtained on the feature map for regression. Finally, position-sensitive ROI pooling is performed on k * k * (C + 1) dimension and 4 * k * k dimension position-sensitive score maps to obtain the corresponding classification and position information.

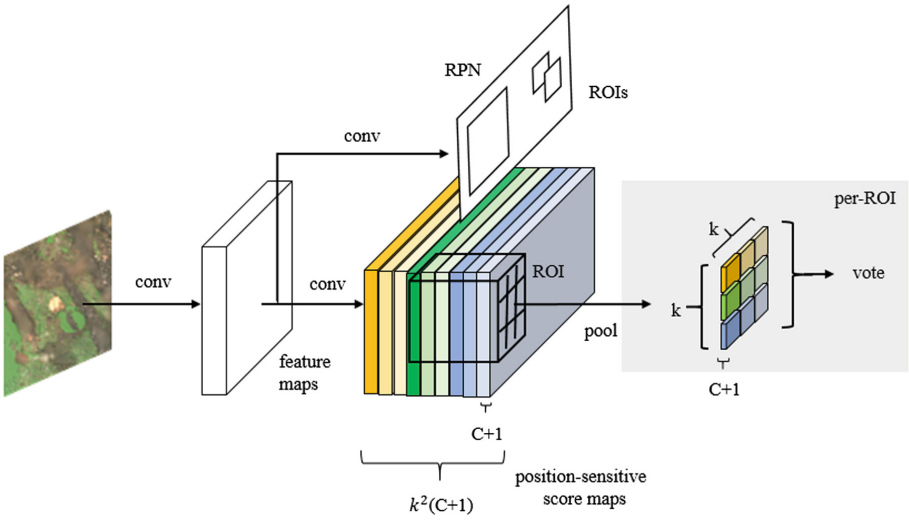

Fig. 7. R-FCN structure

3.2.2 Online Hard Example Mining

According to the loss of input samples, Online Hard Example Mining (OHEM) filters out hard examples to represent the samples that have a greater impact on classification and detection. The obtained hard examples will be trained in stochastic gradient descent. Hard example is selected according to the loss of each ROI and the largest loss ROIs are chosen. The specific operation is to extend the original ROI Network to two ROI Networks, which share parameters. The front ROI Network has only forward operations, mainly for computing losses. The latter ROI Network includes forward and backward operations Hard examples are used as input to calculate the loss and pass back the gradient.

3.2.3 Feature Pyramid Network

Although Faster RCNN has the characteristic of high detection stability, it lacks the ability to detect fine-grained and small-size features. In this paper, a detection framework combining Faster RCNN and FPN (Feature Pyramid Network) is used to obtain

better small object detection results. As shown in Fig. 8(a) shows a sketch of Faster RCNN extracting and predicting features, a process that only uses the last layer feature map of the convolutional neural network. However, due to the small size of spherical wear debris studied in this paper, its information will be lost after several convolution and pooling operations. Figure 8(b) shows the structure of FPN, which uses the inherent multi-scale and multi-level structure of deep convolution neural network and adopts a top-down side connection to construct high-level semantic feature maps at all scales, gaining the ability to detect fine-grained features.

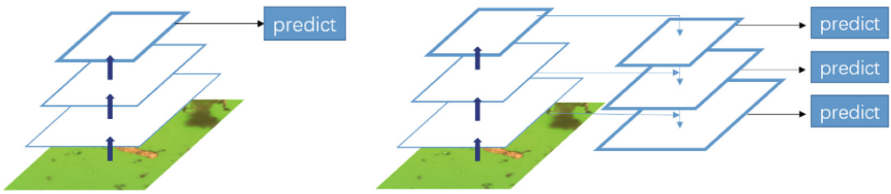

Fig. 8. Different structure of feature map (a) Single feature map (b) Feature pyramid network

3.3 Experiment Analysis

Wear debris detection use original images. The methods of data augmentation in Sect. 2.2.1 is applied. After data augmentation, the training dataset is 2238, both the validation dataset and test dataset are 745. The number of each type of wear debris label bounding boxes are shown in Table 8. In the following experiments, five types of wear debris (fatigue, severe sliding, cutting, spherical, copper) are tested. The learning rate is set to 0.001 with step policy and stepsize is 10000. Max iteration is 20000.

Table 8. Each type of wear debris label bounding boxes

Wear debris	Fatigue	Sever sliding	Cutting	Spherical	Copper
number	1732	1008	1064	3134	1012

Faster RCNN uses ZF, VGG1024, VGG16 and ResNet50 as a pre-trained model to initialize the network parameters. The experiment result uses AP value as evaluating indicator. AP is an indicator of global performance. It is the area value of the Precision-Recall (PR) curve. The formula is shown as Eq. (1).

$$\mathrm{AP} = \int_0^1 P(R)dR \tag{1}$$

Faster RCNN detection results are shown in Table 9. Among these network structures, ResNet50 gets the best effort. ResNet50 trains the deeper network by using

residual modules and conventional SGD. R-FCN use ResNet50 and OHEM compared with Faster RCNN. As illustrated in Table 10, R-FCN with ResNet50 and OHEM gets better test result and shorter test time. In addition, the detection results in Table 9 are based on the framework including only Faster RCNN, and the last three rows in Table 10 are based on the framework including R-FCN, Faster RCNN, OHEM and FPN. Faster RCNN is used to detect the wear debris because the fatigue and severe sliding wear debris have more harm to the normal operation of mechanical equipment.

Table 9. Faster RCNN detection results

Detect model	***mAP***	Fatigue	Severe sliding	Cutting	Spherical	Copper
Faster RCNN+ZF	***0.5812***	0.7099	0.4727	0.7596	0.4458	0.5182
Faster RCNN+VGG1024	***0.6355***	0.7642	0.4976	0.7803	0.4636	0.6717
Faster RCNN+VGG16	***0.7480***	0.7323	0.7698	0.8588	0.5385	0.8403
Faster RCNN+ReNet50	***0.7793***	0.7920	0.8428	0.7734	0.6543	0.8338

Table 10. R-FCN detection results compared with Faster RCNN

Detect model	***mAP***	Fatigue	Severe sliding	Cutting	Spherical	Copper	Test time (sec/img)
Faster RCNN+ ReNet50	***0.7793***	0.7920	0.8428	0.7734	0.6543	0.8338	0.391
Faster RCNN + ReNet101	***0.7700***	0.7677	0.8571	0.8465	0.5293	0.8496	0.180
Faster RCNN+ ReNet101+ FPN+ OHEM	***0.8297***	0.8426	0.8868	0.8844	0.6522	0.8823	0.179
R-FCN+ ReNet50 + FPN + OHEM	***0.8319***	0.7491	0.8512	0.8252	0.8555	0.8787	0.178

According to the detected boxed number, we can get the quantity of each wear debris.

3.4 Grabcut Segmentation on Wear Debris

Graphcut is an image segmentation technology based on graph cut algorithm. It just needs foreground and background input. The algorithm can complete the background and foreground similar supervision weighted graph, and segment image by optimal cutting. Grabcut is the improvement of Graphcut. Grabcut doesn't require user interaction, and it just needs to input foreground region to segment the foreground from the background. The detected boxes in Faster RCNN are input to Grabcut as foreground region. The detected box is shown in Fig. 9. After open operation and close operation, the segmentation result is shown in Fig. 10. The long axis of wear debris can be calculated on the segmented image.

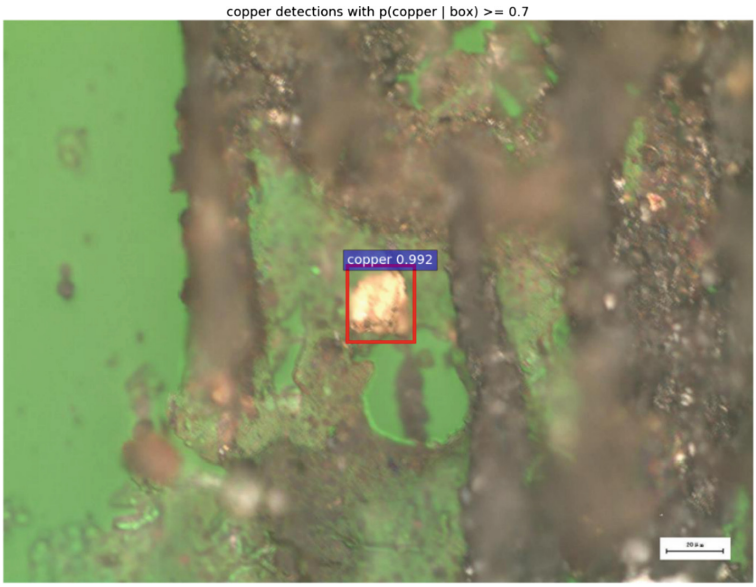

Fig. 9. Faster RCNN detected box in wear debris image

Fig. 10. Grabcut Segmentation result

4 Application

The wear debris in the oil of steel production equipment lubrication system are deposited on the ferrography. Then we use the above methods to analyze the wear debris images, so as to judge the wear degree and failure type of steel equipment and repair it in time.

4.1 Fault Analysis of Caster Ladle Turret Lubricating System

The caster ladle turret bearing of steel plant is the key equipment in the steelmaking production line, and the cost is very high. We evaluated the current wear state of a large ladle turret bearing in a steel plant, and a large number of large size wear debris were found on ferrography of the 4 sample points of the bearing. By analyzing the wear debris images, we find that there were mainly severe sliding and fatigue wear debris, as shown in Fig. 11.

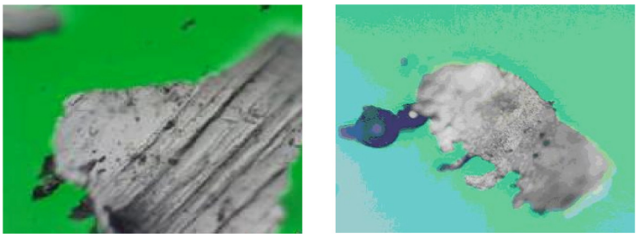

(a) Severe sliding (b) Fatigue

Fig. 11. Wear debris images generated by the bearing

The occurrence of large-size severe sliding wear debris indicates that the sliding wear between the friction pairs is serious. The occurrence of extra-large-size fatigue wear debris indicates that the bearing has a severe fatigue spalling phenomenon. It can be concluded that serious abnormal wear occurs in the bearing. Therefore, it is suggested that the manufacturer prepare as soon as possible so as to replace the bearing. According to the suggestion, the manufacturer disassembled and checked the bearing. The results show that there is a serious fatigue spalling in the main and outer raceway of the bearing, as shown in Fig. 12. The inspection results showed that the fatigue spalling of the bearing had made it unable to continue service, and it further proved that the previous classification results were completely accurate.

(a) Inner main thrust roller fatigue spalling area (b) Outer main thrust roller fatigue spalling area

Fig. 12. Bearing dismantled results

4.2 Fault Analysis of Material Sintering Vibrating Screen Lubricating System

The vibrating screen of steel plant is used to screen ore, with the characteristics of large vibration amplitude and heavy load. The wear debris produced by the vibrator bearing of a vibrating screen in a steel plant. It was found that there were a large number of large size fatigue wear debris on ferrography, as shown in Fig. 13. Therefore, the bearing had serious fatigue wear and tear. It is recommended that the factory arranges the maintenance as soon as possible, and check the bearing damage. After the factory dismantle it, a large number of fatigue spalling were found in the inner ring and rolling body of the free side bearing, as shown in Fig. 14. The cage also had obvious abnormal wear and tear, so the bearing was replaced.

Fig. 13. Fatigue wear debris generated by the bearing

(a) Abnormal wear inner ring of bearing (b) Abnormal wear of rolling body

Fig. 14. Bearing dismantled results

After checking the replacement bearing, it was found that although the prosecution took every 2 d oil change once the measure, but the bearing wear was very large. The wear debris deposited on ferrography were analyzed and we found large size of fatigue wear debris. It indicated that there was still a serious abnormal wear phenomenon in the bearing. Bearing wear status had further deteriorated trend, belonging to the typical fatigue failure. Consequently, the root cause of abnormal wear of the device was not

lubrication, but because of the unreasonable selection of bearings. The factory accordingly redesigned bearing models and replaced all the bearings. By tracking and monitoring the wear debris on ferrography, the new bearing wear rate significantly reduced compared with the original bearing, and the bearing is in good condition.

4.3 Fault Analysis of De-silication Dust Cleaning Fan

The de-silication dust cleaning fan is a tail-wagging equipment for the iron-making production line. Through the ferrographic analysis of sampling the lubrication oil on both sides of motor bearing, it was found that there were a large number of large size wear debris in the load side bearing. Among them, there were normal sliding, fatigue, cutting and spherical wear debris, as shown in Fig. 15. There was serious abnormal wear on the load side bearing, and the main reason for the fault is the wear of the bearing cage. After dismantling the bearing, we found that the motor load side bearing holder was worn by 2–4 mm depth, leaving an obvious indenter, and there was an indentation in the inner ring and outer ring of the bearing. After replacing the bearings on both sides of the motor, the condition of the motor was tested. The vibration of the motor had been restored to the normal level.

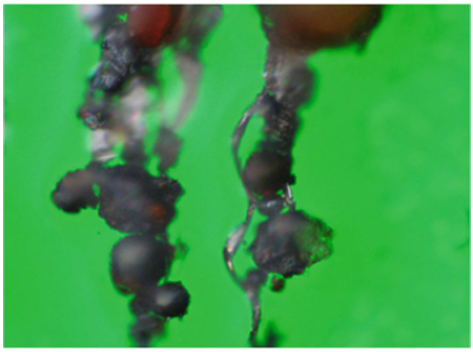

Fig. 15. Wear debris of load side bearing

5 Conclusion and Future Work

In this paper, an improved lightweight CNN UstbNet is proposed. It proves that CNN for the wear debris classification task is very effective. In addition, we use the improved Faster RCNN to detect wear debris and segment wear debris image on detected region proposals through grabcut. The feature pyramid network is added in Faster RCNN to improve the detection result of small objects such as spherical wear debris. The above methods are applied to analyze the fault of caster ladle turret lubricating system, material sintering vibrating screen lubricating system and desilication dust cleaning fan. The application shows that the methods are effective to find the severe wear in steel production equipment.

The UstbNet classification model for single-feature wear debris images has reached a higher classification accuracy, but it still needs to be further improved for multi-feature wear debris images. Future studies will focus more on the classification of multi-feature wear debris images by using multi labels to train the classification model.

Acknowledgment. This work is supported by National key R & D plan (2016YFB0601301), National Natural Science Foundation (51574032, 51674030) and Fundamental Research Funds for the Central Universities (FRF-TP-18-097A1).

References

1. Kun, X., Luxmoore, A.R., Deravi, F.: Comparison of shape features for the classification of wear particles. Eng. Appl. Artif. Intell. **10**, 485 (1997)
2. Zhao, R.: Study on lubrication of metallurgical rolling equipment. Sci. Technol. Enterp. 357–358 (2013)
3. Qin, H., Ren, Z., Zhao, J., Ye, C., Doll, G.L., Dong, Y.: Effects of ultrasonic nanocrystal surface modification on the wear and micropitting behavior of bearing steel in boundary lubricated steel-steel contacts. Wear **392**, 29 (2017)
4. Chang, Z., Jia, Q., Yuan, X., Chen, Y.: Main failure mode of oil-air lubricated rolling bearing installed in high speed machining. Tribol. Int. **112**, 68 (2017)
5. Mosleh, M., Bradshaw, K., Belk, J.H., Waldrop, J.C.I.: Fatigue failure of all-steel and steel-silicon nitride rolling ball combinations. Wear **271**, 2471 (2011)
6. Mao, J.: Study on preparation technology of self-lubricating wear-resistant coatings on mill gear surface by composite of laser cladding and shock peening. Master. Jiangsu University (2016)
7. Wang, F.: Study on the ferrography wear particle with image processing technology. Master. Wuhan University of Technology (2005)
8. Thomas, A.D.H., Davies, T., Luxmoore, A.R.: Computer image analysis for identification of wear particles. Wear **142**, 213 (1991)
9. Stachowla, G.P., Stachowiak, G.W., Podsladlo, P.: Automated classification of wear particles based on their surface texture and shape features. Tribol. Int. **41**, 34 (2008)
10. Roylance, B.J., ALbidewi, I.A., Laghari, M.S., Luxmoore, A.R., Deravi, F.: Computer-aided vision engineering (CAVE)–quantification of wear particle morphology. In: STLE 48th Annual Meeting, Calgary, Alberta, Canada, 6 pp. (1993)
11. Xu, K., Luxmoore, A.R., Jones, L.M., Deravi, F.: Integration of neural networks and expert systems for microscopic wear particle analysis. Knowl.-Based Syst. **11**, 213 (1998)
12. Zuo, H., Wu, Z., Yang, Z.: Application of double BP-network in debris identification. Acta Aeronautica ET Astronautica Sinica **21**, 372 (2000)
13. Li, Q., Zhao, T., Zhang, L., Sun, W., Xi, Z.: Ferrograghy wear particles image recognition based on extreme learning machine. J. Electr. Comput. Eng. **2017**, 1 (2017)
14. Peng, Z.: An integrated intelligence system for wear debris analysis. Wear **252**, 730 (2002)
15. Xiong, A., Kong, X., Wang, J., Chen, D.: The sharable wear particle recognition and wear diagnosis system. Mech. Sci. Technol. Aerosp. Eng. **421**, 421–423 (2002)
16. Peng, Y., Wu, T., Wang, S., Peng, Z.: Wear state identification using dynamic features of wear debris for on-line purpose. Wear **376–377**, 1885 (2017)
17. Yuan, W., Chin, K.S., Hua, M., Dong, G., Wang, C.: Shape classification of wear particles by image boundary analysis using machine learning algorithms. Mech. Syst. Signal Process. **72–73**, 346 (2016)

18. Tian, Y., Wang, J., Peng, Z., Jiang, X.: A new approach to numerical characterisation of wear particle surfaces in three-dimensions for wear study. Wear **282–283**, 59 (2012)
19. Isa, M.C., Yusoff, N.H.N., Nain, H., Yati, M.S.D., Muhammad, M.M., Nor, I.M.: Ferrographic analysis of wear particles of various machinery systems of a commercial marine ship. Procedia Eng. **68**, 345 (2013)
20. Wang, J., Wang, X.: A wear particle identification method by combining principal component analysis and grey relational analysis. Wear **304**, 96 (2013)
21. Wang, H., Huang, R., Gao, L., Wang, W., Xu, A., Yuan, F.: Wear debris classification of steel production equipment using feature fusion and case-based reasoning. ISIJ Int. **58**, 1293 (2018)
22. Wang, J., Zhang, L., Lu, F., Wang, X.: The segmentation of wear particles in ferrograph images based on an improved ant colony algorithm. Wear **311**, 123 (2014)
23. Wu, Z.: An vehicle type recognition method based on Convolution Neural Network. Mech. Electr. Eng. Technol. **Z2**, 608 (2016)
24. Krizhevsky, A., Sutskever, I., Hinton, G.E.: ImageNet classification with deep convolutional neural networks. Commun. ACM **60**, 84 (2017)
25. Yu, S., Jia, S., Xu, C.: Convolutional neural networks for hyperspectral image classification. Neurocomputing **219**, 88 (2017)
26. Ferreira, A., Giraldi, G.: Convolutional Neural Network approaches to granite tiles classification. Expert Syst. Appl. **84**, 1 (2017)
27. Gomez Villa, A., Salazar, A., Vargas, F.: Towards automatic wild animal monitoring: identification of animal species in camera-trap images using very deep convolutional neural networks. Ecol. Inform. **41**, 24 (2017)
28. Dyrmann, M., Karstoft, H., Midtiby, H.S.: Plant species classification using deep convolutional neural network. Biosys. Eng. **151**, 72 (2016)